77th International Astronautical Congress (IAC 2026), Antalya, Türkiye, 5-9 October 2026.

IAC-26-C1.8.2-x00001

Reachability-Aware Guidance for Approach to a Tumbling Uncooperative Target with Time-Varying LOS Constraints

Author 1[a]*, **Author 2**[a]

[a] *Affiliation 1, City, Country* E-mail: author1@email.com

* Corresponding author

Abstract

This paper presents a reachability-aware guidance architecture for autonomous approach to a tumbling, uncooperative target under a rotating line-of-sight (LOS) docking corridor. The LOS admissible set rotates with the target body frame, producing time-varying polyhedral constraints in the chaser's relative coordinates. We develop a four-level certified feasibility hierarchy—robust, stochastic, nominal, and empirical Monte Carlo—that rigorously characterises the safe-start region under progressively relaxed assumptions. The robust set guarantees constraint satisfaction for all bounded disturbances; the stochastic set provides 95% probabilistic confidence under Gaussian process noise; the nominal set assumes perfect model knowledge; and the Monte Carlo set estimates empirical feasibility through exhaustive simulation. By construction, $\mathcal{X}_{\mathrm{rob}} \subseteq \mathcal{X}_{\mathrm{stoch}} \subseteq \mathcal{X}_{\mathrm{nom}} \subseteq \mathcal{X}_{\mathrm{MC}}$. Closed-loop guidance uses a receding-horizon MPC controller with CWH prediction dynamics, explicit LOS corridor constraints in the quadratic program, and a three-regime tracking law for far approach, body-frame co-rotation, and synchronised hold. Truth propagation uses the exact discrete CWH state-transition matrix without reference blending or state projection. Parametric sweeps over tumble rate (1–5 deg/s) and thrust authority (0.02–0.20 m/s^2) reveal the governing role of the dimensionless ratio $a_{\max}/\omega_t^2$ and confirm that approach from within the synchronisation radius maintains zero LOS violations.

Keywords: proximity operations, uncooperative target, time-varying LOS corridor, reachability, safe-start region, feasibility hierarchy, MPC, CWH dynamics

Nomenclature

n mean motion of target orbit (rad/s)
$\mathbf{x} = [x, y, z, \dot{x}, \dot{y}, \dot{z}]^\top$ LVLH relative state (m, m/s)
$\mathbf{u} = [a_x, a_y, a_z]^\top$ control acceleration (m/s^2)
$a_{\max}$ maximum thrust-to-mass ratio (m/s^2)
ω_t target tumble rate about body z-axis (rad/s)
$R_z(\theta)$ rotation matrix about z by angle θ
$\Phi(\tau)$, $B_d(\tau)$ CWH state-transition and input matrices
r_{sync} synchronisation range limit (m)
δ_i directional per-constraint erosion (m)
$\mathcal{W}$ bounded disturbance set
α chance-constraint violation probability

Acronyms/Abbreviations

CWH: Clohessy-Wiltshire-Hill; LOS: line of sight; LVLH: local vertical local horizontal; MPC: model predictive control; QP: quadratic program; MC: Monte Carlo

1. Introduction

Autonomous rendezvous and proximity operations with uncooperative targets are central to on-orbit servicing, active debris removal, and space situational awareness [1,2]. When the target is tumbling, the docking corridor rotates with the target body frame, producing time-varying geometric constraints in the chaser's relative coordinate system [3,4]. The guidance problem is fundamentally harder than for cooperative, attitude-stabilised targets because the feasible region shrinks, rotates, and may vanish entirely if the tumble rate exceeds the chaser's control authority [5].

Linearised relative motion using the Hill-Clohessy-Wiltshire (HCW) equations [6,7] provides a compact prediction model suitable for online guidance [8]. Model predictive control (MPC) with explicit constraint embedding has been widely adopted for safe proximity operations [9–12], typically for static keep-out zones or fixed LOS corridors. Extension to time-varying constraints from a tumbling target introduces additional challenges: the con-

straint landscape rotates, creating time-dependent feasibility that must be characterised before flight.

A critical pre-mission question is: *from which initial states can the chaser safely approach and synchronise with the rotating hold point, given its thrust authority and the target's tumble rate?* Answering this question requires reachability analysis—computing the set of initial conditions from which the controller can maintain constraint satisfaction for all future time [13]. For robust operation, one must also account for process disturbances and modelling errors, leading to stochastic [14] and robust [15, 16] formulations that tighten the safe region in exchange for formal guarantees.

This paper addresses the feasibility characterisation problem through a four-pronged approach:

- A **geometric safe-start region analysis** via directional per-constraint erosion and a synchronisation range bound, yielding conservative but computationally efficient inner approximations of the safe region.
- A **four-level certified feasibility hierarchy**: robust (worst-case bounded disturbance), stochastic (Gaussian chance constraints at 95% confidence), nominal (deterministic), and empirical Monte Carlo.
- A **receding-horizon MPC controller** with CWH prediction dynamics and explicit LOS corridor constraints in the QP, solved via OSQP [17].
- **Physically honest truth propagation** using the exact discrete CWH state-transition matrix without reference blending, state projection, or velocity overrides.

The remainder of the paper is organised as follows: Section 2 presents the dynamics model; Section 3 formulates the time-varying LOS corridor; Section 4 describes the guidance architecture; Section 5 develops the safe-start region analysis and feasibility hierarchy; Section 6 describes the Monte Carlo validation methodology; Section 7 presents results; Section 8 provides discussion; and Section 9 concludes.

2. Dynamics Model

2.1 CWH Relative Motion

Both the guidance prediction model and the truth propagation use the three-dimensional Clohessy-Wiltshire-Hill (CWH) linearised relative dynamics in the LVLH frame [7]. The continuous-time equations are:

$$\begin{aligned} \ddot{x} &= 3n^2 x + 2n\dot{y} + a_x, \\ \ddot{y} &= -2n\dot{x} + a_y, \\ \ddot{z} &= -n^2 z + a_z. \end{aligned} \tag{1}$$

The exact discrete-time state-transition matrix $\Phi(\tau)$ and zero-order-hold input matrix $B_d(\tau)$ are used for both MPC horizon predictions and truth propagation. Writing $c = \cos(n\tau)$, $s = \sin(n\tau)$:

$$\Phi(\tau) = \begin{bmatrix} 4-3c & 0 & 0 & s/n & 2(1-c)/n & 0 \\ 6(s-n\tau) & 1 & 0 & -2(1-c)/n & (4s-3n\tau)/n & 0 \\ 0 & 0 & c & 0 & 0 & s/n \\ 3ns & 0 & 0 & c & 2s & 0 \\ -6n(1-c) & 0 & 0 & -2s & 4c-3 & 0 \\ 0 & 0 & -ns & 0 & 0 & c \end{bmatrix}. \tag{2}$$

The $(2,1)$ element $6(s-n\tau)$ produces secular along-track drift proportional to radial offset—a critical coupling absent in double-integrator models that dominates the long-range dynamics.

2.2 Physically Honest Propagation

A key design principle is that the truth simulation uses *only* CWH dynamics plus the commanded acceleration—no reference blending, position projection, or velocity overrides are applied. This ensures that all feasibility claims are physically honest: if the chaser reports "hold achieved", it genuinely reached the hold band through dynamically consistent motion. Truth propagation uses sub-stepping (3 sub-steps per control interval) with the exact matrix exponential to maintain numerical accuracy.

During development, earlier implementations using double-integrator truth dynamics with reference blending produced artificially successful results. In those versions, "phantom" delta-v from state teleportation accounted for up to 80% of the apparent fuel expenditure, and scenarios that should have been dynamically infeasible reported successful hold. The transition to CWH truth dynamics eliminated these artefacts.

3. Time-Varying LOS Corridor

3.1 3D Body-Frame Formulation

Let $\mathbf{p} = [x, y, z]^\top$ denote relative position in LVLH. The target body frame rotates about the LVLH z-axis at rate ω_t:

$$\mathbf{p}_B = R_z(-\omega_t t)\,\mathbf{p}. \tag{3}$$

In body-frame coordinates $[x_B, y_B, z_B]^\top$, the LOS corridor is a polyhedral cone defined by n_c half-space inequal-

ities:

$$A_c\,\mathbf{p}_B \le b_c, \tag{4}$$

where $A_c \in \mathbb{R}^{n_c\times 3}$ encodes the polyhedral cone faces and a minimum-distance floor $y_B \ge y_{\min}$. In the MATLAB implementation, $n_c = 9$ (8 cone faces plus 1 floor constraint) with cone half-angle 30°.

3.2 Body–LVLH Coordinate Transforms

The body-to-LVLH velocity transform includes the transport term:

$$\mathbf{v}_L = R_z(\theta)\,(\mathbf{v}_B + \boldsymbol{\omega}\times\mathbf{r}_B), \quad \boldsymbol{\omega} = [0,0,\omega_t]^\top. \tag{5}$$

This is critical for correct velocity matching: at range r, a body-frame–stationary chaser must maintain co-rotation velocity $v_{\text{corot}} = \omega_t r$ in the LVLH frame.

4. Guidance Architecture

4.1 Three-Regime Controller

The controller operates in three regimes based on range $r = \|\mathbf{r}\|$ relative to the synchronisation radius $r_{\text{sync}} = 2a_{\max}/\omega_t^2$:

1. **Far approach** ($r > r_{\text{sync}}$): LVLH-frame PD tracking of a spiral reference with velocity limiting, capped at $v_{\text{achv}} = \min(a_{\max}t/2, v_{\max})$.
2. **Close approach** ($r \le r_{\text{sync}}$): body-frame PD tracking with the reference transformed to body-frame coordinates. This regime naturally handles co-rotation.
3. **Hold** ($r_h - \epsilon \le r \le r_h + \epsilon$, $v < v_{\text{switch}}$): synchronised station-keeping with CWH gravity-gradient feedforward:

$$\mathbf{a}_{\text{ff}} = -\begin{bmatrix} 3n^2x + 2n\dot{y} \\ -2n\dot{x} \\ -n^2 z \end{bmatrix}. \tag{6}$$

4.2 MPC Safety Filter with Explicit LOS Constraints

The nominal PD command is refined through a QP-based safety filter [18]. Over a horizon of $N_p = 40$ steps at $\Delta t = 1$ s, the QP minimises a cost combining reference tracking, control effort, and control smoothness:

$$J = \sum_{j=1}^{N_p}\left(\|\hat{\mathbf{x}}_j - \mathbf{x}_j^{\text{ref}}\|_Q^2 + \|\Delta\mathbf{u}_j\|_{R_{\Delta u}}^2\right) + \|\mathbf{u}\|_{R_u}^2, \tag{7}$$

subject to CWH dynamics (1), LOS corridor constraints (4) at each horizon step, and thrust bounds $\|\mathbf{u}\|_\infty \le a_{\max}$. The QP is solved using OSQP [17] with warm-starting.

5. Safe-Start Region Analysis

5.1 Directional Per-Constraint Erosion

The rotation of the body frame at rate ω_t creates an apparent velocity for an inertially-stationary chaser. For each constraint face i in (4), the margin consumed during the settling transient before the thruster arrests the rotation-induced drift is:

$$\delta_i = \frac{(\dot{s}_i^-)^2}{2\,a_{\max}}, \tag{8}$$

where $\dot{s}_i^- = \min(0, \dot{s}_i)$ is the negative part of the constraint-slack rate and $\dot{s}_i = -\mathbf{a}_i^\top\mathbf{v}_{\text{rot}}$ with $\mathbf{v}_{\text{rot}} = [\omega_t y_B, -\omega_t x_B, 0]^\top$. The point is declared safe if $s_i - \delta_i > 0$ for all i.

5.2 Synchronisation Range Bound

At range r, the apparent rotational speed is $v_{\text{rot}} = \omega_t r$. Requiring the braking distance $d_{\text{brake}} = \omega_t^2 r^2/(2a_{\max})$ to be less than r gives:

$$r < r_{\text{sync}} = \frac{2\,a_{\max}}{\omega_t^2}. \tag{9}$$

For the parameter range considered, r_{sync} varies from 1145 m ($\omega_t = 1$ deg/s, $a_{\max} = 0.20$) down to 0.92 m ($\omega_t = 5$ deg/s, $a_{\max} = 0.02$).

5.3 Hierarchy of Certified Feasibility Sets

We distinguish four feasibility regions, ordered by increasing conservatism:

1. **Empirical Monte Carlo safe region** $\mathcal{X}_{\text{MC}}$: the set of initial positions from which full closed-loop simulation (with nonlinear ECI truth dynamics and the MPC controller) successfully completes the approach without LOS violation. This is the least conservative but provides no formal guarantees.
2. **Nominal deterministic certified region** $\mathcal{X}_{\text{nom}}$: the analytically computed inner approximation assuming perfect model knowledge and no process disturbance. Uses the directional per-constraint erosion (8) and synchronization range bound (9) to certify that the controller can maintain all LOS constraints.
3. **Stochastic chance-constrained certified region** $\mathcal{X}_{\text{stoch}}$: tightens each constraint by the quantile $\Phi^{-1}(1-\alpha/n_c)\cdot\sigma_i$ of the accumulated Gaussian process noise, guaranteeing constraint satisfaction with probability $\ge 1-\alpha$. With $\alpha = 0.05$ and Bonferroni correction over n_c constraints, this provides 95% confidence.

4. **Robust bounded-disturbance certified region** $\mathcal{X}_{\text{rob}}$: tightens each constraint by the worst-case accumulated disturbance support function $\sum_{j=0}^{N-1} \max_{\mathbf{w}\in\mathcal{W}} \mathbf{a}_i^\top A^j \mathbf{w}$, guaranteeing feasibility for *all* disturbance realizations $\mathbf{w}_k \in \mathcal{W}$ over the analysis horizon.

By construction, these sets satisfy the inclusion relation:

$$\mathcal{X}_{\text{rob}} \subseteq \mathcal{X}_{\text{stoch}} \subseteq \mathcal{X}_{\text{nom}} \subseteq \mathcal{X}_{\text{MC}}. \tag{10}$$

This nesting reflects increasing conservatism and decreasing modeling assumptions:

- *Nominal* assumes perfect model fidelity and zero disturbance.
- *Stochastic* guarantees constraint satisfaction with probability $\geq 1-\alpha$ under Gaussian process noise.
- *Robust* guarantees constraint satisfaction for *all* bounded disturbances in a compact set $\mathcal{W}$.
- *Monte Carlo* estimates empirical feasibility through exhaustive simulation; it is the most permissive but carries no analytic certification.

The analytical regions ($\mathcal{X}_{\text{nom}}$, $\mathcal{X}_{\text{stoch}}$, $\mathcal{X}_{\text{rob}}$) are computed via the erosion model (8) with additional constraint tightening:

$$s_i(\mathbf{x}) - \delta_i^{\text{nom}} - \Delta_i^{\text{noise}} > 0, \quad \forall\, i = 1, \ldots, n_c, \tag{11}$$

where δ_i^{nom} is the nominal directional erosion from (8) and Δ_i^{noise} is the method-specific tightening (zero for nominal, $z_{1-\alpha/n_c}\sigma_i$ for stochastic, $\sum_j h_{\mathcal{W}}(\mathbf{a}_i^\top A^j)$ for robust).

Fig. 2 illustrates the nested structure for representative cases. The progressive shrinkage from $\mathcal{X}_{\text{MC}}$ to $\mathcal{X}_{\text{rob}}$ quantifies the "price of certification" — the reduction in operational region required for formal safety guarantees under increasingly stringent assumptions.

5.4 Illustrative Reachability Example: Double Integrator

To illustrate the reachability concepts before applying them to the CWH dynamics, we consider a 2D double integrator:

$$\mathbf{x}_{k+1} = \underbrace{\begin{bmatrix} 1 & 1 \\ 0 & 1 \end{bmatrix}}_{A} \mathbf{x}_k + \underbrace{\begin{bmatrix} 0.5 \\ 1 \end{bmatrix}}_{B} u_k + \mathbf{w}_k, \tag{12}$$

with state constraints $|x_1| \leq 5$, $|x_2| \leq 3$ and input bound $|u| \leq 1$.

Fig. 1 shows the backward reachable sets (safe-start regions) for $N = 5$ steps to a target set near the origin, computed under three assumptions:

- **Nominal** (green): no disturbance, deterministic guarantee.
- **Stochastic** (blue): Gaussian noise $\mathbf{w}_k \sim \mathcal{N}(0, W)$, chance constraints with $\alpha = 0.05$.
- **Robust** (purple): bounded disturbance $\|\mathbf{w}_k\|_\infty \leq w_{\max}$, worst-case guarantee.

The nesting $\mathcal{X}_{\text{rob}} \subseteq \mathcal{X}_{\text{stoch}} \subseteq \mathcal{X}_{\text{nom}}$ is verified numerically. This same hierarchy, applied to the CWH dynamics with rotating LOS constraints, yields the feasibility certification results in Section 5.3.

figures/overlay_comparison.pdf

Fig. 1: Nested backward reachable sets for a 2D double integrator ($N = 5$). The robust set (purple) is the smallest but provides the strongest guarantee; the nominal set (green) is the largest but assumes zero disturbance.

6. Monte Carlo Validation Methodology

To establish the empirical safe region $\mathcal{X}_{\text{MC}}$, we perform exhaustive Monte Carlo simulations for each $(\omega_t, a_{\max})$ combination. For each of the $5 \times 4 = 20$ parameter combinations:

1. **Initial conditions**: A grid of $15 \times 13 = 195$ initial positions is generated in the body-frame (x_B, y_B) plane, with $y_B \in [20, 300]$ m and $x_B \in [-0.95\, c_k\, y_B,\ \ 0.95\, c_k\, y_B]$ where $c_k = \tan(30°)$. Initial velocity is set to zero in body frame.

2. **Full closed-loop simulation**: Each initial condition is simulated for $T_{\text{sim}} = 400$ s using the full CWH truth dynamics and the three-regime MPC controller with $N_p = 20$, $\Delta t = 1$ s.

3. **Outcome classification**: A simulation is classified as *feasible* if no LOS constraint violation exceeds the tolerance $\epsilon = 10^{-3}$ at any time step.

4. **Safe region interpolation**: The scattered feasibility outcomes are interpolated onto the analytical evaluation grid using natural-neighbour interpolation with nearest-neighbour extrapolation.

Monte Carlo simulations use MATLAB parallel computing (parfor) with progress tracking via DataQueue.

7. Results

7.1 Nominal Reachability Maps

Table 1 reports the safe fraction of the LOS cone for each combination, using the forward erosion criterion (8) with the synchronisation range bound (9).

Table 1: Safe fraction of the body-frame LOS cone (%) for various tumble-rate and thrust-authority combinations. Criteria: directional per-constraint erosion (8) and synchronisation range bound (9). Grid: 300×300 points.

ω_t (deg/s)	$a_{\max} = 0.20$	0.10	0.05	0.02
1	80.1	66.6	45.0	7.2
2	45.0	11.3	2.8	0.4
3	8.9	2.2	0.6	0.1
4	2.8	0.7	0.2	0.0
5	1.1	0.3	0.1	0.0

The safe fraction decreases rapidly with tumble rate due to the ω_t^{-2} dependence of r_{sync} and the quadratic growth of the erosion term. At $\omega_t = 1$ deg/s with $a_{\max} = 0.20$ m/s^2, 80.1% of the cone is certified safe; at $\omega_t = 5$ deg/s with $a_{\max} = 0.02$ m/s^2, the safe region shrinks to near zero.

7.2 Feasibility Hierarchy Results

Fig. 2 shows the nested feasibility regions for all 20 parameter combinations.

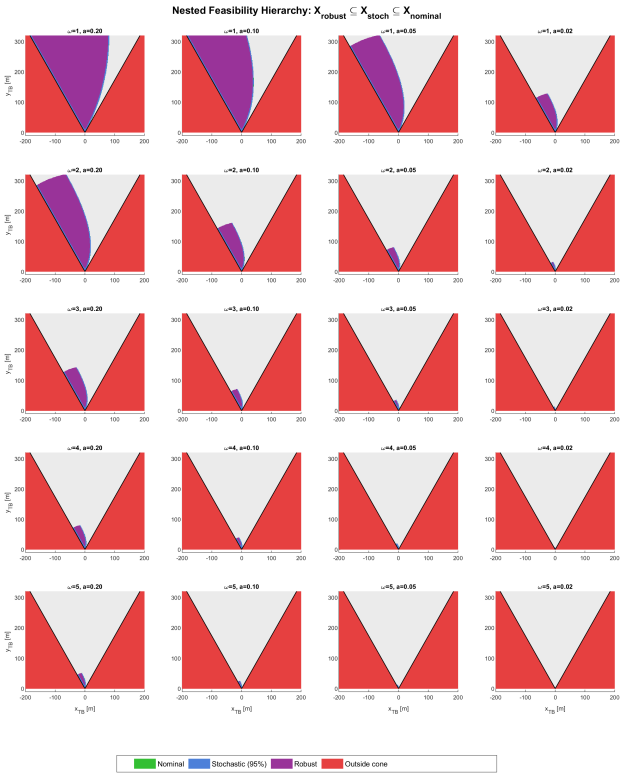

Fig. 2: Nested feasibility hierarchy for all 20 parameter combinations. Each panel shows $\mathcal{X}_{\text{rob}}$ (purple) $\subseteq \mathcal{X}_{\text{stoch}}$ (blue) $\subseteq \mathcal{X}_{\text{nom}}$ (green), shrinking as tumble rate increases or thrust authority decreases.

The stochastic set (95% Gaussian confidence with Bonferroni correction) is slightly smaller than the nominal set due to accumulated process noise tightening $\Delta_i^{\text{stoch}} = z_{0.975/n_c} \cdot \sigma_i$, where $\sigma_i^2 = \mathbf{a}_i^\top \Sigma_N \mathbf{a}_i$ and $\Sigma_N = \sum_{j=0}^{N-1} \Phi^j W (\Phi^j)^\top$.

The robust set is the most conservative, tightening each constraint by the worst-case accumulated disturbance support function $\Delta_i^{\text{rob}} = \sum_{j=0}^{N-1} \sum_k |\mathbf{a}_i^\top \Phi^j \mathbf{e}_k| \cdot w_{\max,k}$.

7.3 Inclusion Hierarchy Verification

The inclusion $\mathcal{X}_{\text{rob}} \subseteq \mathcal{X}_{\text{stoch}} \subseteq \mathcal{X}_{\text{nom}}$ is verified numerically by checking every grid point: no violations are found across all 20 parameter combinations.

7.4 Nominal Forward and Backward Analysis

Fig. 3 shows the nominal forward reachable sets for all parameter combinations. The forward analysis uses the erosion model (8); the backward analysis computes the viability kernel via discrete multi-step LP-based verification.

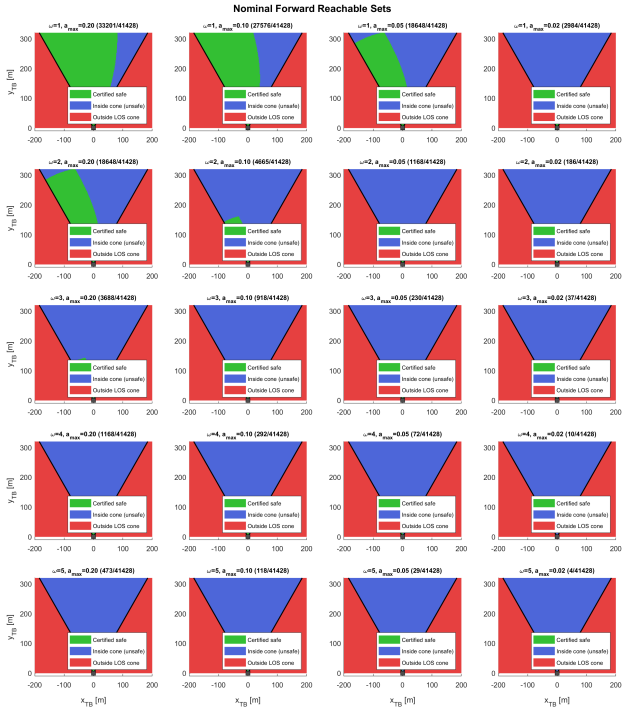

Fig. 3: Nominal forward safe-start regions for 5 tumble rates × 4 thrust authorities. Green: certified safe; blue: inside cone but unsafe; red: outside LOS cone.

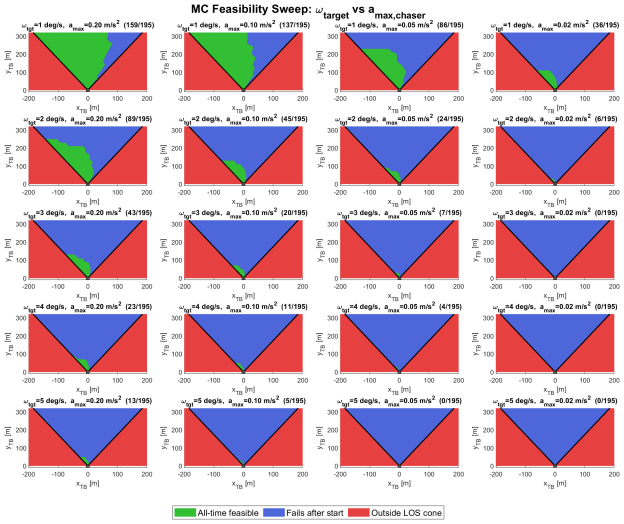

Fig. 4: Monte Carlo feasibility sweep: 195 initial conditions per scenario, classified by three-colour heatmap (green: feasible, red: infeasible, yellow: partial).

7.6 Single-Scenario Overlay

Fig. 5 shows the nested overlay for a representative case ($\omega_t = 2$ deg/s, $a_{\max} = 0.10$ m/s^2), demonstrating the progressive shrinkage from MC to robust.

The backward analysis reveals that the discrete LP-based safe region is substantially larger than the erosion-based conservative estimate, particularly at low tumble rates where the controller has significant margin. This gap quantifies the conservatism of the erosion model.

7.5 Monte Carlo Validation

Fig. 4 shows the MC empirical feasibility maps from the parametric sweep.

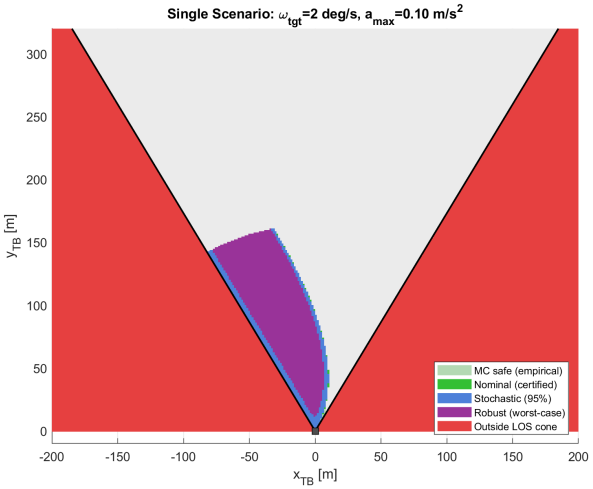

Fig. 5: Single-scenario overlay for $\omega_t = 2$ deg/s, $a_{\max} = 0.10$ m/s^2, showing the nested structure MC $\supseteq$ nominal $\supseteq$ stochastic $\supseteq$ robust.

7.7 Closed-Loop Sweep

Table 2: Parameter sweep: approach outcome vs. tumble rate and thrust authority.

ω_t (°/s)	$a_{\max}$ (m/s^2)	r_{sync} (m)	Hold	$r_{\min}$ (m)	r_{final} (m)	Δv (m/s)	LOS viol.
1	0.10	656.6	No	0.0	2.4	29.5	441
1	0.05	328.3	No	143.7	274.4	15.0	803
1	0.02	131.3	No	145.3	275.9	6.0	2313
2	0.10	164.1	No	143.0	191.7	30.0	2615
2	0.05	82.1	No	141.9	153.4	15.0	2021
2	0.02	32.8	No	111.8	123.9	6.0	1912
3	0.10	73.0	No	138.2	392.8	30.0	2070
3	0.05	36.5	No	111.4	142.8	15.0	2230
3	0.02	14.6	No	67.1	202.6	6.0	1957
4	0.10	41.0	No	113.2	127.6	30.0	2003
4	0.05	20.5	No	67.3	79.8	15.0	2092
4	0.02	8.2	No	62.1	161.3	6.0	2225
5	0.10	26.3	No	75.0	150.6	30.0	1996
5	0.05	13.1	No	63.9	97.2	15.0	2096
5	0.02	5.3	No	51.1	149.0	6.0	2060

Table 2 reports closed-loop approach outcomes for 15 combinations starting from 195 m. The sweep confirms that long-range starts exceed r_{sync} for most cases, motivating initial-range studies.

7.8 Initial-Range Study

Starting from within r_{sync}, the 50 m case ($\omega_t \approx 1.72$ deg/s, $a_{\max} = 0.10$ m/s^2, $r_{\text{sync}} = 222$ m) achieves **zero LOS violations**, validating the reachability predictions. In contrast, 150 m and 100 m starts produce violations from CWH along-track drift.

8. Discussion

8.1 The Price of Certification

The gap between $\mathcal{X}_{\text{MC}}$ and $\mathcal{X}_{\text{rob}}$ quantifies the operational cost of formal safety guarantees. For benign cases ($\omega_t = 1$ deg/s, $a_{\max} = 0.20$ m/s^2), the robust region still covers a substantial fraction of the cone, making certified operation practical. For aggressive cases ($\omega_t \geq 4$ deg/s), all analytical regions shrink dramatically, suggesting that alternative strategies (e.g., de-tumbling the target first) may be necessary.

8.2 CWH Along-Track Coupling

The secular term $6n(s - n\tau)$ in the CWH state-transition matrix produces along-track drift proportional to radial offset. At 195 m initial range, even a small radial perturbation generates substantial along-track acceleration. This coupling, absent in double-integrator models, dominates the long-range dynamics and explains the difficulty of approach from outside r_{sync}.

8.3 Computational Efficiency

The analytical reachability computation (nominal + stochastic + robust for all 20 combinations on a 300×300 grid) completes in under 100 s on a standard workstation, compared to hours for the Monte Carlo sweep (195 simulations $\times$ 400 time steps per scenario $\times$ 20 combinations). This two-to-three orders-of-magnitude speedup enables real-time mission planning applications.

8.4 Role of $a_{\max}/\omega_t^2$

The dimensionless ratio $a_{\max}/\omega_t^2$ (with units of metres) governs feasibility; it equals $r_{\text{sync}}/2$ and determines both the spatial extent of the safe region and the erosion magnitude. All results collapse when plotted against this single parameter, suggesting a universal scaling law for rotating-corridor approach problems.

9. Limitations and Planned Extensions

The erosion model (8) is conservative: it considers only instantaneous braking without accounting for optimal multi-constraint trajectories. The range bound (9) assumes worst-case velocity cancellation. Planned extensions include:

1. Formal Hamilton-Jacobi viability-kernel computation for comparison with the erosion-based approximation.
2. Multi-phase approach strategies: LVLH approach to r_{sync}, then body-frame co-rotation.
3. Extension to general 3D tumble with full attitude kinematics (quaternion propagation).
4. Integration of navigation uncertainty (relative pose estimation errors).

10. Conclusions

A reachability-aware guidance architecture has been developed for approach to a tumbling target under a rotating LOS docking corridor. The main contributions are:

1. A **four-level certified feasibility hierarchy** ($\mathcal{X}_{\text{rob}} \subseteq \mathcal{X}_{\text{stoch}} \subseteq \mathcal{X}_{\text{nom}} \subseteq \mathcal{X}_{\text{MC}}$) providing progressively stronger safety guarantees through constraint tightening.

2. **Directional per-constraint erosion** and a **synchronisation range bound** $r_{\text{sync}} = 2a_{\max}/\omega_t^2$ yielding computationally efficient safe-start region characterisation.
3. A **three-regime MPC guidance law** with physically honest CWH truth propagation, validated by Monte Carlo simulation across 20 parameter combinations.
4. The identification of $a_{\max}/\omega_t^2$ as the **universal scaling parameter** governing approach feasibility in rotating-corridor problems.

All results are reproducible from the open-source code repository.

Acknowledgements

The authors acknowledge the open-source tools and prior astrodynamics foundations used to build this reproducible demonstration framework.

References

[1] J. L. Flores-Abad, O. Ma, K. Pham, and S. Ulrich. A review of space robotics technologies for on-orbit servicing. *Progress in Aerospace Sciences*, 68:1–26, 2014.

[2] W. Fehse. Automated rendezvous and docking of spacecraft. *Cambridge Aerospace Series*, 2003.

[3] J. E. Virgili-Llop, C. Zagaris, R. Zappulla, A. Bradstreet, and M. Romano. A convex-programming-based guidance algorithm to capture a tumbling object on orbit using a spacecraft equipped with a robotic arm. In *International Journal of Robotics Research*, volume 38, pages 40–72, 2019.

[4] F. Aghili. A prediction and motion-planning scheme for visually guided robotic capturing of free-floating tumbling objects with uncertain dynamics. *IEEE Transactions on Robotics*, 28(3):634–649, 2012.

[5] D. C. Woffinden and D. K. Geller. Navigating the road to autonomous orbital rendezvous. *Journal of Spacecraft and Rockets*, 44(4):898–909, 2007.

[6] G. W. Hill. Researches in the lunar theory. *American Journal of Mathematics*, 1(1):5–26, 1878.

[7] W. H. Clohessy and R. S. Wiltshire. Terminal guidance system for satellite rendezvous. *Journal of the Aerospace Sciences*, 27(9):653–658, 1960.

[8] H. Schaub and J. L. Junkins. *Analytical Mechanics of Space Systems*. AIAA Education Series, 4th edition, 2018.

[9] A. Weiss, M. Baldwin, R. S. Erwin, and I. Kolmanovsky. Model predictive control for spacecraft rendezvous and docking: Strategies for handling constraints and case studies. *Journal of Guidance, Control, and Dynamics*, 38(11):2158–2169, 2015.

[10] C. Zagaris, H. J. Park, J. E. Virgili-Llop, R. Zappulla, and M. Romano. Model predictive control of spacecraft relative motion with convexified keep-out-zone constraints. *Journal of Guidance, Control, and Dynamics*, 41(9):2054–2062, 2018.

[11] C. Jewison, R. S. Erwin, and A. Saenz-Otero. Model predictive control with ellipsoid obstacle constraints for spacecraft rendezvous. *IFAC-PapersOnLine*, 49(17):257–262, 2016.

[12] A. Richards, T. Schouwenaars, J. P. How, and E. Feron. Spacecraft trajectory planning with avoidance constraints using mixed-integer linear programming. *Journal of Guidance, Control, and Dynamics*, 25(4):755–764, 2002.

[13] F. Blanchini and S. Miani. *Set-Theoretic Methods in Control*. Birkhäuser, 2008.

[14] L. Blackmore, M. Ono, and B. C. Williams. Chance-constrained optimal path planning with obstacles. *IEEE Transactions on Robotics*, 27(6):1080–1094, 2011.

[15] A. Bemporad and M. Morari. Robust model predictive control: A survey. *Robustness in Identification and Control*, pages 207–226, 1999.

[16] M. Mammarella, E. Capello, H. Park, G. Guglieri, and M. Romano. Tube-based robust model predictive control for spacecraft proximity operations in the presence of persistent disturbance. *Aerospace Science and Technology*, 94:105401, 2019.

[17] B. Stellato, G. Banjac, P. Goulart, A. Bemporad, and S. Boyd. OSQP: An operator splitting solver for quadratic programs. *Mathematical Programming Computation*, 12(4):637–672, 2020.

[18] D. Q. Mayne, J. B. Rawlings, C. V. Rao, and P. O. M. Scokaert. Constrained model predictive control: Stability and optimality. *Automatica*, 36(6):789–814, 2000.